International Forum on Aeroelasticity and Structural Dynamics
IFASD 2019
9-13 June 2019, Savannah, Georgia, USA

ACTIVE CONTROL FOR NONLINEAR AEROELASTIC SYSTEMS

Shakir Jiffri[1], Hamed H. Khodaparast[1], Marinos Manolesos[1], and Sebastiano Fichera[2]

[1] College of Engineering, Swansea University (Bay Campus)
Fabian Way, Crymlyn Burrows, Swansea SA1 8EN, Wales, United Kingdom
shakir.jiffri@swansea.ac.uk
h.haddadkhodaparast@swansea.ac.uk
marinos.manolesos@swansea.ac.uk

[2] School of Engineering, University of Liverpool
Brownlow Hill, Liverpool L69 3GH, England, United Kingdom
sebastiano.fichera@liverpool.ac.uk

Keywords: nonlinearity, aeroelasticity, active control, feedback linearisation

Abstract: The dynamic responses to aeroelastic gusts/manoeuvres play an important part across much of the design and development of an aircraft and have an impact upon structural design, aerodynamic characteristics, weight, flight control system design, control surface design, and performance. They determine the most extreme stress levels, fatigue damage, and damage tolerance for a particular design. To this end, there has been great interest in efficient loads alleviation in aircraft structures.

The ultimate aim of this project is to study the dynamic behaviour of a nonlinear aeroelastic system due to gust loads, and to investigate the use of linear/nonlinear active control with the aim of mitigating vibrations in the system, and reducing the aerodynamic loads that would, in the real world, be introduced into the airframe. The present paper discusses the authors' existing research which will serve as the foundation for the aforementioned aim of the project. Implementation of techniques such as partial feedback linearisation, the combination in real-time of simulation-based and experimentally measured data during control – which we envisage will play a vital role in the current project – are addressed, including results of closed-loop control of a pitch-plunge aerofoil. As the present research is ongoing – and any significant results are yet to be generated – this paper will present briefly the current status and next steps planned for the project.

1 INTRODUCTION

The development of effective simulation and experimental techniques for the control of aircraft has for long been a continuous pursuit. The push towards greener, lighter, efficient aircraft has never been stronger. Consequently, it is becoming increasingly important to improve modelling methods and challenge what may be unsound conventions and simplifications made in the past, either due to pragmatism or lack of suitable methods to handle the complexity of problems that would otherwise have arisen. Nonlinearity is one such area, whose effects are becoming increasingly evident as we move along the trends described above. Detailed literature reviews of nonlinearity in aeroelasticity were carried out by Dowell et al. [1] and Lee et al. [2]. Furthermore, several publications on the application of active control on aeroelastic systems have appeared. Of closer relevance to the present work is the

research carried out by Strganac and colleagues [3-8], in which the application of active control on aeroelastic systems with hardening-type structural nonlinearities has been investigated both theoretically also experimentally, through the use of quasi-steady aeroelastic models. These studies utilised the feedback linearisation nonlinear control method, in conjunction with LQR control as the linear control objective. Motivated by the findings of these works, the authors in [9] presented (a) the real-time use of a low-order numerical model which enables the inclusion of unsteady aerodynamic effects (improving model accuracy) in the control process of an aeroelastic system, and the ability of the controller to completely eliminate a fully developed limit cycle oscillation (LCO), and (b) the use of pole-placement as the linear control objective, which, although more challenging to implement experimentally, has advantages over LQR control such as providing the user more flexibility in adjusting specific dynamic parameters, and removing the need to determine appropriate weighting factors that are required in LQR control.

The present work seeks to progress the research in [9] by using a flexible wing instead of a pitch-plunge aerofoil, and also including the effects of gust inputs. In the past few decades, many different methods have been proposed for the prediction of gust loads, including worse-case scenarios. Potozoky and Zeiler [10] obtained identical results with two computationally efficient methods, the matched filter theory (MFT) and the random process theory. Kanda and Dowell [11] later demonstrated that the MFT although efficient, produced results nearly twice as large as those calculated with the "1-cos" gust approach determined by the CS-25 regulations. More recent approaches focus on stochastic surfaces [12] and optimization techniques [13] to improve the efficiency of the identification of critical loads. In [14], the effects of structural non-linearities and uncertainties were studied using a two-dimensional aeroelastic model with cubic non-linear heave and pitch springs. [15] considers the effects of local structural nonlinearities on the worst-case prediction of gust loads.

The authors of the present article seek to address the need to develop improved methods to control aeroelastic response in realistic systems (e.g. flexible wings), under realistic environmental conditions (e.g. including the effects of gusts). Knowledge and experience from the authors' own previous research, and other relevant research will be drawn upon in this endeavor. The present paper discusses some of this relevant research - which will provide a firm foundation for the next phase of research - and towards the end of the paper a brief outline of the current status and next plans will be given.

2 EXPERIMENTAL SETUP

The rig pertaining to the experimental work discussed in this paper was a two degree-of-freedom pitch-plunge aerofoil section, mounted in a low-speed wind tunnel at the University of Liverpool (Figure 1). The wind tunnel test section dimensions are 1.2 m × 0.4 m × 1.0 m, with a maximum achievable speed of around 18 m/s. A dSPACE real-time control system is utilised for closed-loop control. The inputs to dSPACE are the displacements and velocities of pre-defined locations on the aerofoil, as depicted in Figure 2, measured using laser sensors. The output from dSPACE, once amplified, drives a twin piezo-stack arrangement [16, 17] which actuates a trailing edge flap on the aerofoil. Stepped-sine modal testing of the aeroelastic system is achieved using an LMS SCADAS III system. Prior to the main experiments, it was verified that the flexible modes of the aeroelastic system are substantially higher in frequency than those of the pitch-plunge modes, and also that the chosen values of pitch and plunge stiffnesses gave rise to a flutter speed that was achievable within the air speed range of the wind tunnel. Furthermore, the parameters of the numerical model were tuned to match those of the experimental system.

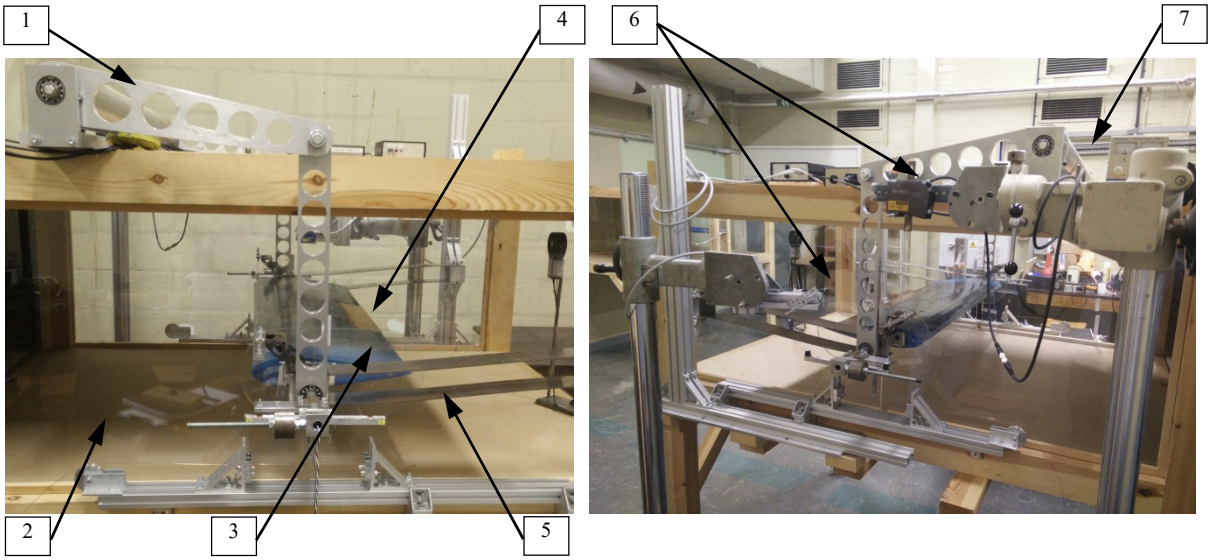

(a) Wind tunnel test section – view 1 (LHS)

(b) Wind tunnel test section – view 2 (RHS)

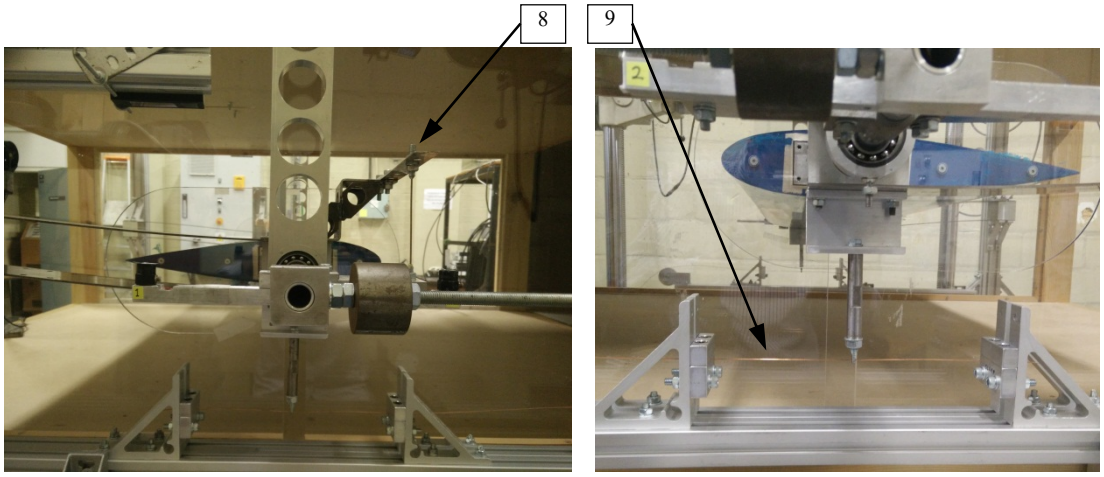

(c) Wind tunnel test section – view 3 (RHS)

(d) Tensioned wire design for plunge nonlinear stiffness

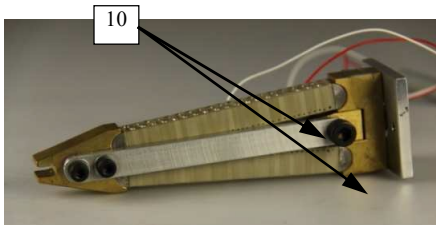

(e) V-stack trailing edge flap actuator

(1) aerofoil vertical support
(2) housing
(3) aerofoil section
(4) trailing edge control surface
(5) plunge spring - linear
(6) laser displacement sensors
(7) torsion bar
(8) pitch spring
(9) plunge spring - nonlinear
(10) piezo-stack actuators
(located inside (4))

Figure 1: Aeroelastic system experimental setup.

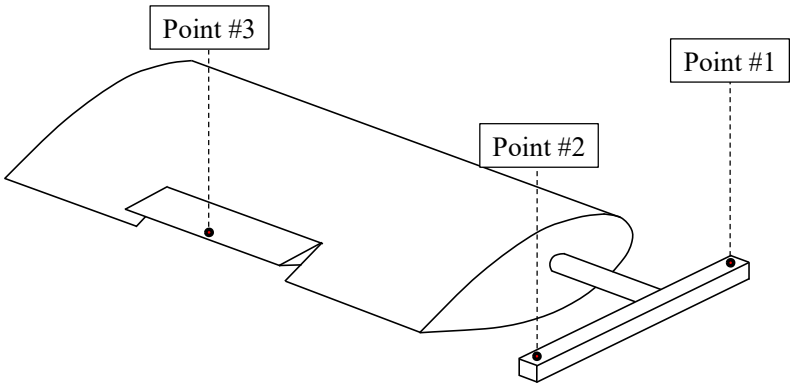

Figure 2: Measurement locations on aeroelastic system.

The aerofoil section has a NACA 0018 profile, with a chord length of 0.35 m and a span of 1.2 m. It is equipped with a trailing edge flap, located centrally, having chord-wise and span-wise dimensions 25% and 35%, respectively, with respect to aerofoil chord and span. The flap is capable of rotating approximately ±5˚, up to a bandwidth of approximately 15 Hz. Adjustable leaf springs provide stiffness to the aerofoil, independently in the plunge and pitch directions. A structural nonlinearity is incorporated into the system in the form of a hardening polynomial stiffness in the plunge degree-of-freedom. This is achieved by the clamped-clamped tensioned wire arrangement depicted in Figure 1(d). The force-displacement relationship may be expressed as

$$F_{nl} = K_{\xi} h + K_{\xi_3} h^3 + K_{\xi_5} h^5, \tag{1}$$

where all coefficients K of the various powers of the plunge term h are positive. The flap is the only means of input to the system during closed-loop control, and it is actuated by a mechanically amplified "V-stack" piezoelectric stack arrangement [16, 17] as depicted in Figure 1(e). The control law computes the required action by the flap, based on pitch and plunge deflections and velocities, and also aerodynamic states (addressed later) of the aerofoil section. The controller then outputs the appropriate voltage signal from dSPACE, which once amplified, is directed to the piezo-stacks in the V-stack actuator, causing rotation of the flap.

3 NUMERICAL MODEL, PARAMETER TUNING AND RESPONSE COMPARISON

A twelve-state numerical model with four structural and eight aerodynamic states was employed in this work. The aerofoil section shown in Figure 3 has two degrees of freedom that define the motion about a reference elastic axis (e.a.). The plunge deflection is denoted by *h*, positive downward, and α is the angle of attack about the elastic axis, positive with nose up. The motion is restrained by two springs, of stiffness K_{ξ} and K_{α}, and is assumed to have a horizontal equilibrium position at $h = \alpha = 0$. Structural damping in both degrees of freedom was also included in the system. A trailing-edge flap, assumed massless in this study, was used in combination with an active control system as the input to the aeroelastic system.

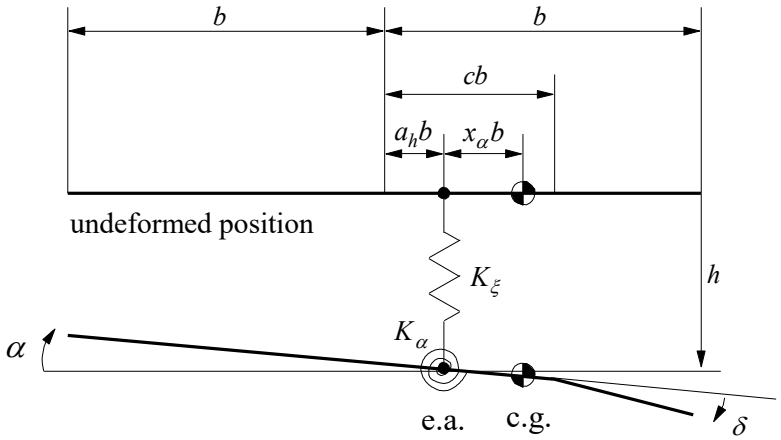

Figure 3: Schematic of a two-degree of freedom aeroelastic system;
the wind velocity is to the right and horizontal.

The motion of the system, without control surface dynamics and with a linear structural model, is described in non–dimensional form by

$$\begin{bmatrix} \tilde{m} & \frac{x_\alpha}{r_\alpha^2} \\ x_\alpha & 1 \end{bmatrix} \begin{Bmatrix} \xi'' \\ \alpha'' \end{Bmatrix} + \begin{bmatrix} \frac{2\zeta_\xi \bar{\omega}}{U^*} & 0 \\ 0 & \frac{2\zeta_\alpha \bar{\omega}}{U^*} \end{bmatrix} \begin{Bmatrix} \xi' \\ \alpha' \end{Bmatrix} + \begin{bmatrix} \left(\frac{\bar{\omega}}{U^*}\right)^2 & 0 \\ 0 & \left(\frac{1}{U^*}\right)^2 \end{bmatrix} \begin{Bmatrix} \xi \\ \alpha \end{Bmatrix} = \begin{Bmatrix} -\frac{1}{\pi\mu} C_L(\tau) \\ \frac{2}{\pi\mu r_\alpha^2} C_m(\tau) \end{Bmatrix}. \tag{2}$$

The lift coefficient, C_L, is defined positive upward according to the usual sign convention in aerodynamics. The plunge displacement is positive downward. Hence the negative sign in front of C_L in eq. (2). Note also that the above equations are formulated in terms of a non–dimensional time, τ, based on the aerofoil semi–chord and freestream speed, $\tau = tU/b$. The prime notation $(\bullet)', (\bullet)''$, used herein, indicates differentiation with respect to non-dimensional time τ, instead of the well-known dot notation which is often used to denote differentiation with respect to absolute time t. The above model of the pitch–plunge aerofoil system, with an appropriate model of the aerodynamics, was used in this work to simulate the dynamics of the nonlinear aeroelastic test rig. Theoretical detail on the aerodynamics used in this model including its mathematical formulation have been derived previously [18]. The end result is an aeroelastic model that approximates the unsteady aerodynamic behaviour using additional state variables. The coupled model consists of 12 state variables, 8 of which are aerodynamic states required to model the unsteady aerodynamics as described above, and the remaining 4 which are structural states. The trailing–edge flap rotation is used as control input. The coupled system of equations, with the dependence on non-dimensional time τ omitted for brevity, may be cast in the nonlinear state-space form

$$\mathbf{x}' = \mathbf{f}(\mathbf{x}) + \mathbf{g}u, \tag{3}$$

where detail on the structure of the equation may be found in [9]. The term $\mathbf{f}(\mathbf{x})$ is a nonlinear function of the state vector $\mathbf{x}$, and u represents the flap rotation δ. This allows one to setup the numerical model starting from the baseline aeroelastic parameters of the pitch–plunge aerofoil described later on.

The parameters of the numerical model were set to the values acquired from wind tunnel tests. Subsequently, fine tuning of these parameters was performed such that the discrepancy between both the linear and nonlinear dynamic behaviour of the numerical model and the aeroelastic system was minimised. Table 1 contains the finalised parameter values, where the format in which they are presented follows that used by [19, 20] and many others.

Table 1: Aeroelastic model parameter values.

Parameter	Value	Parameter	Value	Parameter	Value
ω_α (rad/s)	29.13955	a	-0.32571	ζ_α	0.0115
r_α	0.5	c	0.5428	$\tilde{m} = m_{pln}/m_{rot}$	2.21669
x_α	0.021	b (m)	0.175	β_{ξ_3}	1085.62
ω_ξ (rad/s) (linear/nonlinear)	24.64246 / 26.41656	μ	30	$\beta_{\xi_5}, \beta_{\alpha_3}, \beta_{\alpha_5}$	0
$\bar{\omega}$ (linear/nonlinear)	0.84567 / 0.90655	ζ_ξ	0.0175		

The non-dimensional nonlinearity coefficients $\beta_{\xi_3}, \beta_{\xi_5}, \beta_{\alpha_3}, \beta_{\alpha_5}$ are derived from eq. (1), knowing the semi-chord b. The different values for ω_ξ (and $\bar{\omega}$) in the linear and nonlinear cases arises from the tensioned wire design of the nonlinear structural stiffness described earlier. When the tensioned wire is attached to the aerofoil, in addition to the nonlinear terms, a component of linear stiffness is also introduced. It is this additional linear stiffness that increases ω_ξ (and therefore $\bar{\omega}$) in the underlying linear behaviour of the nonlinear system.

A combination of methods was employed during acquisition of the aeroelastic system's parameters (see [9] for details). The responses simulated using the measured parameters, for both linear and nonlinear cases were compared with the respective measured responses from the aeroelastic system. The overall tuning objective then was to make adjustments to the measured parameters so as to reduce the model/aeroelastic system discrepancies both in the linear and nonlinear cases. During initial tuning attempts, it was noted that some of the requirements were conflicting, therefore a compromise between satisfying linear and nonlinear response matching was required. The final tuned set of parameters was decided upon once such a good balance was deemed to have been achieved.

3.1 Linear case - Frequency domain tests

In the absence of the tensioned-wire nonlinearity, the variation of natural frequencies and damping ratios with airspeed was simulated, and subsequently compared with the actual values obtained through modal tests. Stepped sine modal testing was performed between speeds 0 and 14.5 m/s, at intervals of 1 m/s in most cases. The testing was performed in two configurations; in the first case the flap was used as the input, whereas in the second case an electromagnetic shaker was used instead of the flap. In both cases, the displacements at points #1 and #2 (Figure 2) were chosen as outputs. FRF data was post-processed to extract the natural frequencies and damping ratios. The results between simulation and experiment are compared in Figure 4. The predicted linear flutter speed (LFS) is 19.42 m/s, marked by the vertical dashed line. Evidently, there is a small but noticeable discrepancy between measured

and predicted damping values, especially for the pitch mode. This can be attributed largely to the fact that the finalised parameter set seeks to represent a complicated physical system by a simplified model that, among numerous uncertainties, neglects freeplay and frictional nonlinearities in the connection between the nose of V-stack actuator and the flap.

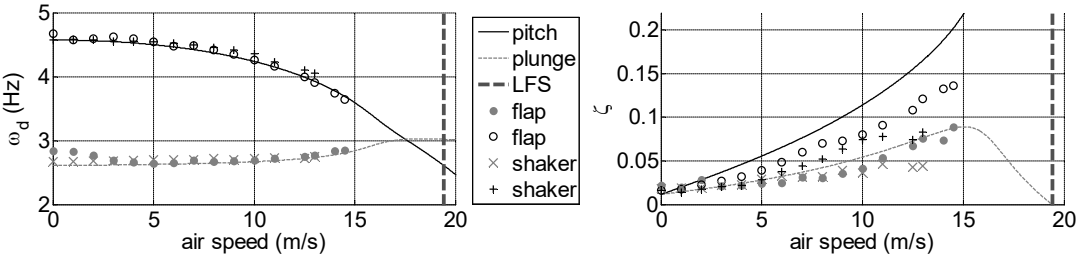

Figure 4: Variation of ω_d and ζ with airspeed..

3.2 Nonlinear case – Phase portrait plots of LCO

With the tensioned-wire nonlinearity included, the aeroelastic system was simulated at an airspeed of 15 m/s under an initial condition of $\xi = 0.05$, with all other states set to zero. An LCO was reached once the transient motions decayed. The simulated result was then compared with the response from the experimental rig. A comparison between the phase portrait diagrams for the experimental and simulated LCO responses is shown in Figure 5.

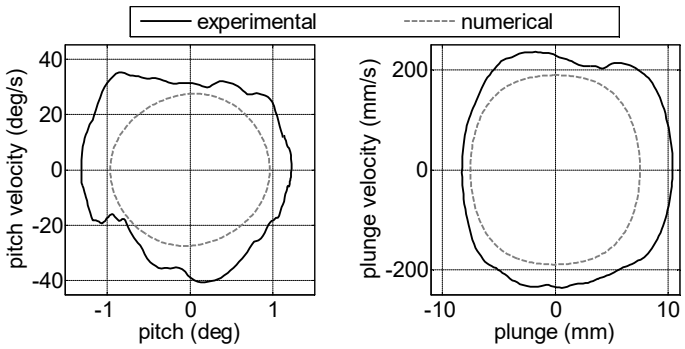

Figure 5: Phase portrait of physical states at U = 15 m/s.

It is evident from the above figure that there is good agreement between the aeroelastic system and the tuned numerical model, notwithstanding the apparent presence of additional harmonics in the experimental pitch phase portrait plot. Again, frictional and free-play effects in the aeroelastic system – absent in the numerical simulation – would partly contribute to the discrepancies observed.

4 REAL-TIME USE OF NUMERICAL MODEL IN THE CONTROL LOOP

The control laws applied in the aeroelastic system were synthesised from the 12-state numerical model described earlier. When implemented, the state-feedback controller requires access to all 12 states in real-time. The 4 structural states were obtained from direct measurement of pitch and plunge, and their time derivatives. The remaining 8 aerodynamic states were not measured directly; it therefore became necessary to acquire them by other means. This objective was fulfilled by embedding the numerical model in the experimental

control loop and utilising it to generate in real time the aerodynamic states. The measured flap deflection angle – i.e. the physical implementation of the input to the aeroelastic system - was directed to the embedded numerical model, which then generated in real-time the full 12-state vector. The first 4 entries of this vector – i.e. the structural states – were then replaced by the measured values to create a "hybrid" state vector which was the basis on which the control input was computed. The hybrid vector was then fed back into the embedded numerical model (along with the flap deflection angle) which allowed computation of the state vector at the next time step. Figure 6 depicts a simplified schematic of the control strategy described herein. An explanation of the purpose/function of each block is now given, where it should be noted that the numbering does not necessarily reflect the sequence of steps.

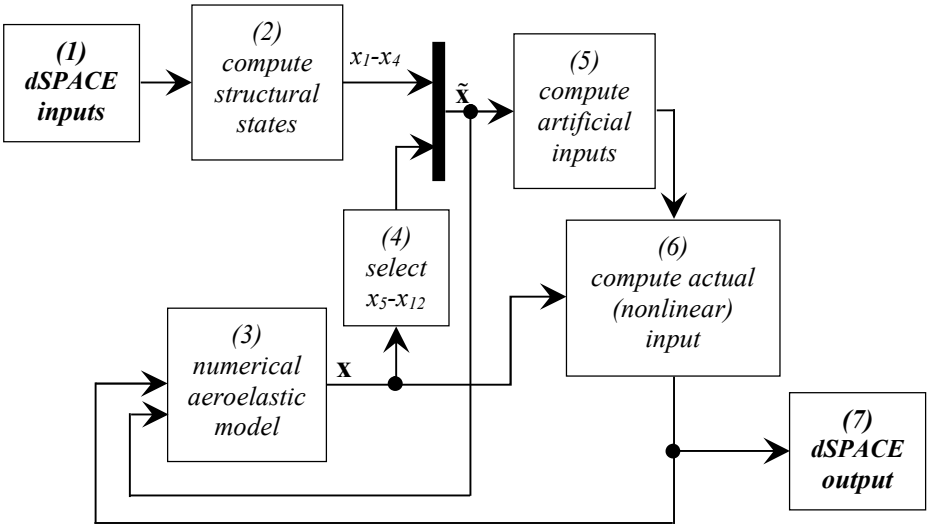

Figure 6: Schematic of control strategy

(1) The displacements at points #1, #2 and #3 from the three laser displacement sensors (Figure 2) are read into dSPACE, and passed through second-order Butterworth low-pass filters to remove noise.
(2) The displacements at points #1 and #2 are converted into pitch angle (rad) and non-dimensional plunge ξ, then differentiated with respect to time to compute velocities.
(3) The flap rotation angle δ is computed through knowledge of pitch angle, plunge displacement and the displacement at point #3.
(4) The embedded numerical model generates the full state vector $\mathbf{x}$ based on knowledge of the measured structural states $x_1 - x_4$ and also the actual flap rotation δ.
(5) The aerodynamic states $x_5 - x_{12}$ are picked from the full state vector $\mathbf{x}$ generated by the embedded numerical model.
(6) Once the measured structural states $x_1 - x_4$ are combined with the numerical aerodynamic states $x_5 - x_{12}$ to form the new "hybrid" state vector $\tilde{\mathbf{x}}$, the artificial inputs ([18]) are computed
(7) The actual, nonlinear input is computed
(8) The output from dSPACE is sent to the piezoelectric actuator of the flap to effect the required rotation.

The time step between measurements is 0.001 seconds, which is determined by dSPACE. Thus, the embedded numerical model and, in fact, the entire control loop depicted in Figure 6 are evaluated once every 0.001 seconds. This time interval is adequately small to ensure a smooth variation of the state variables that are computed by the model through numerical integration.

5 RESULTS – ACTIVE CONTROL IMPLEMENTED

Once adequate confidence of the ability of the tuned numerical model to replicate the dynamics of the experimental system at various airspeeds was gained, active control was implemented. The pitch degree-of-freedom was chosen as the output to base the partial feedback linearisation on. Prior to implementation, it was necessary to assess the stability of the internal dynamics resulting from pitch output linearisation. This was carried out, and the resulting analysis [9] showed that the internal dynamics were indeed stable.

5.1 Pole-placement via feedback linearisation

The control aim is set to suppress LCO by eliminating the underlying nonlinearities in the system. This was achieved by applying a controller that provides linearising feedback to cancel out the nonlinear behaviour of the system. As for the linear part of the controller, it was sought to modify the dynamics of the controlled pitch sub-system by applying pole-placement. Specifically, the pole-placement objective was to increase the damping in the pitch system. With the system undergoing LCO, the controller was implemented with a desired value of the pitch damping ratio (ζ_{CL}) specified. Figure 7 shows the pitch and plunge responses for $\zeta_{CL} = 0.3$, where the controller was switched on at exactly 3 seconds. The associated flap motion is shown in Figure 8.

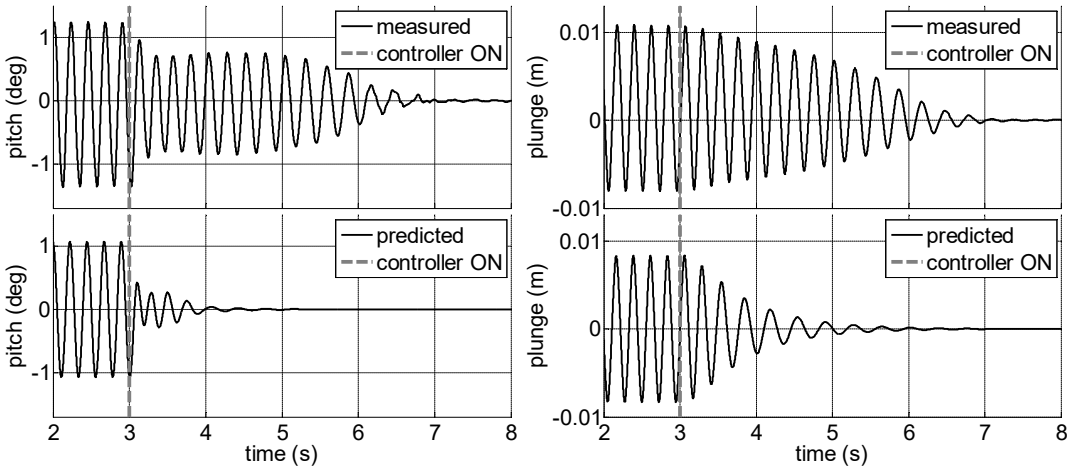

Figure 7: Closed-loop response of aeroelastic system for $\zeta_{CL} = 0.3$, at U = 15 m/s.

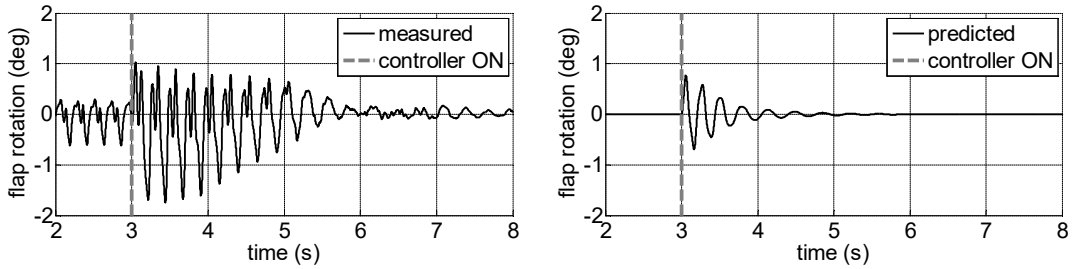

Figure 8: Flap motion for closed-loop control of aeroelastic system for $\zeta_{CL} = 0.3$, at U = 15 m/s.

It is evident that once activated, the controller successfully suppresses the LCO and drives the response to the origin in just under 5 seconds. Repeatability of the above behaviour was verified by carrying out the same test multiple times and ensuring a consistent outcome. In the

simulated responses shown in the bottom half of Figure 7, the effect of the Butterworth low-pass filters has been included for consistency when comparing with experimental measurements. A comparison of the measured responses with the predicted ones – where the controller is activated at the same point along a given cycle as in the experimental case, for consistency in comparison - yields that in the latter case, significantly less time is required for the response to decay. A variety of reasons may be contemplated for the discrepancy, such as the loss of accuracy during computation of pitch and plunge deflections, introduction of noise during numerical differentiation of pitch and plunge to obtain respective velocities etc. Also, it was confirmed using offline numerical simulations that the phase delays resulting from filtering of signals required for numerical differentiation etc. played a small, but significant role in causing this discrepancy. Another major source of discrepancy could be attributed to the mismatch between the tuned and actual system parameters, resulting in the dynamics not being cancelled out completely as desired. Consequently, complete uncoupling of the pitch motion from the remaining dynamics is not achieved; this is reflected in the nature of the measured pitch motion where content from multiple modes of vibration is evident. However, one may conclude from inspecting the actual closed-loop response that the extent of this problem is not so great as to prevent the present control method from being implemented with satisfactory effectiveness. The closed-loop control was repeated several times for different damping ratios. Figure 9 shows the variation of decay time as a function of assigned damping ratio ζ_{CL}, where decay time has been defined as the time for the pitch and plunge response magnitudes to decay to 0.02˚ (≈1.5% of LCO amplitude) and 0.1 mm (≈1% of LCO amplitude) respectively, from the moment the controller is switched on.

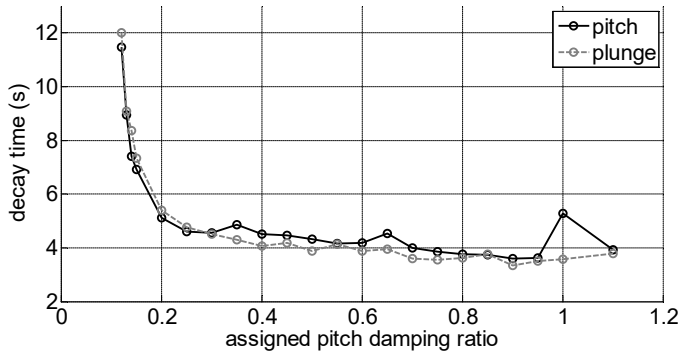

Figure 9: Variation of decay time in closed-loop response with assigned pitch damping ratio, at U = 15 m/s.

For values of ζ_{CL} ranging from zero to around 0.11, the controller failed to suppress LCO. However, as seen in Figure 9, for $\zeta_{CL} > 0.12$, the LCO is suppressed completely. It is interesting to note that the rate of decrease in decay time between around $0.12 < \zeta_{CL} < 0.2$ is much higher than for subsequent values. It was observed during the experiment that for higher values of ζ_{CL} the flap actuator motion consisted of higher amplitude high frequency components, and therefore operated in a more arduous regime as compared with smaller ζ_{CL}. Therefore, given the above trend in the decay time variation, it is appropriate to assign a damping value approximately between $0.2 < \zeta_{CL} < 0.4$.

6 MOVING TOWARDS IMPLEMENTATION IN A FLEXIBLE WING UNDER GUST LOADS

6.1 Introduction

The techniques and general approach utilised in the experimental work discussed in the above sections are being extended to the MODFLEX [21] flexible wing, which will be mounted in the Swansea University low-speed wind tunnel (Figure 10), and tested in the presence of gust loads. This section provides a description of the work envisaged in continuing this research, followed by a brief account of progress to date and next steps.

Figure 10: Swansea University low-speed wind tunnel.

6.2 Work Description

The next phase of this research will involve both simulation and experimental components. The modular “aerofoil sector” based design of the MODFLEX wing will allow relatively easy changing of configuration, such that various control configurations may be tested (e.g. SISO, MIMO involving either a single or multiple sectors). Control inputs to the system will be provided through Trailing edge and/or Leading edge flaps actuated by brushless DC motors.

Initially, the open-loop structural and aeroelastic dynamic behaviour of the wing will be characterised through modal tests, and experimental results from the tests will be used to update the associated numerical model of the wing to ensure it represents the actual dynamic behaviour of the wing. A structural nonlinearity in the built-in end will then be introduced, and the resulting nonlinear system also experimentally and numerically characterised.

The work then goes on to explore the application of active aeroelastic control techniques via the trailing and/or leading-edge control surfaces, in the presence of gusts. The numerical model will be valuable in narrowing down the control configurations to those most effective, which may then be implemented in the actual rig. The control aim is set to reduce the aerodynamic loads due to gust encounter, whilst assigning closed-loop dynamics to the system (damping, natural frequencies), for which a partial feedback linearisation based approach will be used.

6.3 Progress to date

The construction of the flexible wing model, including the actuated sector with both leading and trailing edge flaps has been completed (Figure 11). Maxon ECX16 brushless DC motors with GPX gearheads have been acquired, and mounted in the actuated sectors, one each to rotate the trailing and leading edge flaps (Figure 12 (b)). Each motor will be controlled through a dSPACE MicroLabBox system (Figure 13 (a)), via Maxon's own ESCON 50/5 servo-contoller (Figure 12 (a)), driving each motor. A Data Physics ABACUS system has been acquired (Figure 13 (b)) which will be used for frequency domain tests of the rig.

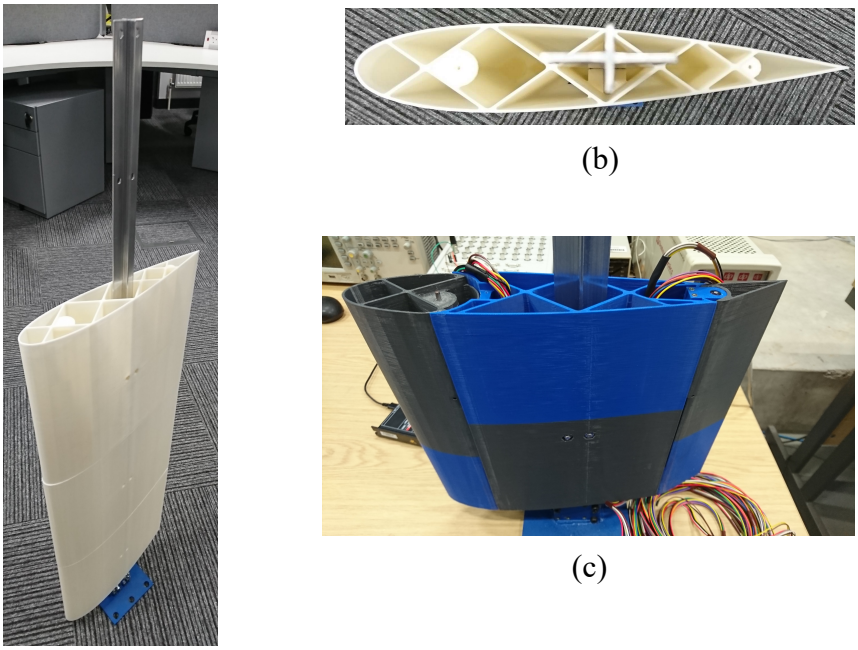

(a) (b) (c)

Figure 11: MODFLEX wing: (a) passive sectors (b) cross-section (c) actuated sector

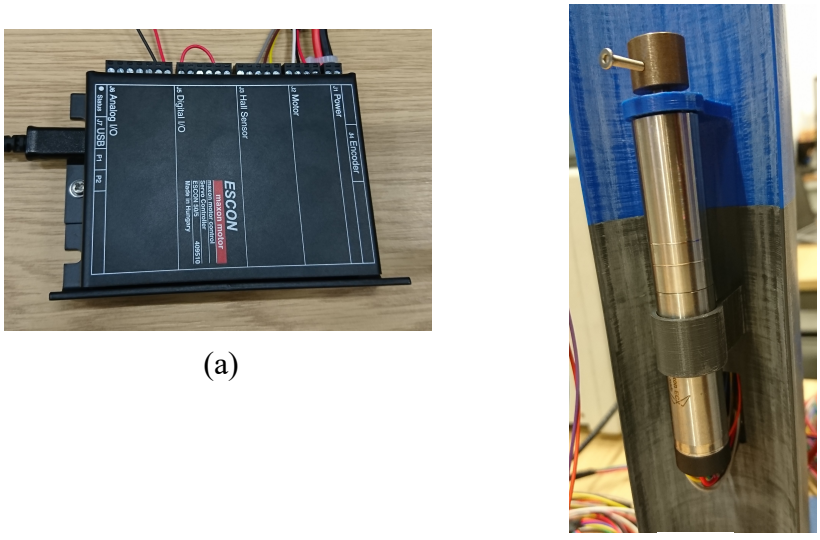

(a) (b)

Figure 12: (a) ESCON 50/5 servocontroller (b) Maxon ECX16 brushless DC motor with gearhead

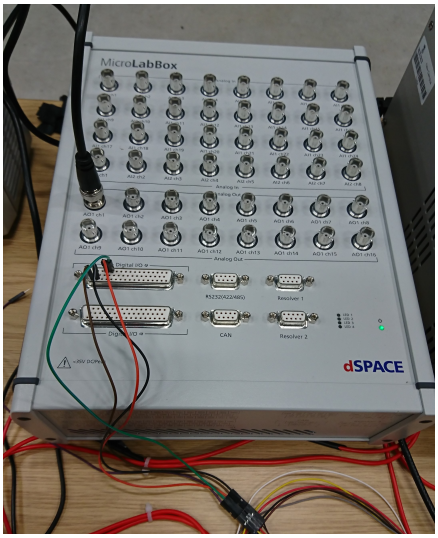

(a)

(b)

Figure 13: (a) dSPACE MicroLabBox (b) Data Physics ABACUS system.

6.4 Next Steps

The Swansea University wind tunnel is a new facility (constructed in 2015-16), and it is only since recently that it is being utilised significantly. At present, the flow at speeds less than around 10 m/s is not sufficiently steady. Once this issue has been resolved, the first major test will be to acquire from experimental FRF measurements the variation of natural frequency and damping ratio of the bending and torsional modes of the wing, across a range of pre-flutter airspeeds. This data will be used to update the associated numerical model, which will then be used to trial a variety of control methods and configurations, from which the most relevant for experimentation may be decided upon. The next phase will likely be the implementation of linear active control methods, using the trailing and/or leading edge as input. Progressing from here onwards, an appropriate design for the inclusion of a structural nonlinearity will be sought, upon completion of which nonlinear active control methods (such as the aforementioned partial feedback linearisation) will be implemented.

Running in parallel with the above, the design (and eventual manufacture) of a gust generator system is being actively discussed within our research group at Swansea. The design used at the University of Bristol [22], or similar, is being considered at present. Once manufactured, the active control methods outlined above will be tailored to account for the gust inputs.

The results from the above experiments and simulations will provide valuable insight into the effectiveness of the methods, and also provide direction for further research.

7 CONCLUSIONS

This paper has discussed the implementation of partial feedback linearisation to control the dynamics of a structurally nonlinear pitch-plunge aeroelastic system from the authors' recent research. Results confirm that the approach of combining simulation-based and experimentally measured data in real-time during active control is capable of yielding high-quality closed-loop response; this will prove valuable in the next phase of the research, where certain state variables are either difficult or impossible to measure during experiments. The

partial feedback linearisation method combined with pole-placement has been shown to be a reliable and effective approach in the elimination of LCO, and also in changing the dynamics of the underlying linear system as desired. These two major components, in addition to other experience gained, will be fundamental in progressing simulation and experiments with the MODFLEX flexible wing, eventually with gust loads included.

8 REFERENCES

[1] Dowell, E., J. Edwards, and T. Strganac, *Nonlinear aeroelasticity.* Journal of Aircraft, 2003. **40**(5): p. 857-874.

[2] Lee, B.H.K., S.J. Price, and Y.S. Wong, *Nonlinear aeroelastic analysis of airfoils: bifurcation and chaos.* Progress in Aerospace Sciences, 1999. **35**(3): p. 205-334.

[3] Ko, J., A.J. Kurdila, and T.W. Strganac, *Nonlinear control of a prototypical wing section with torsional nonlinearity.* Journal of Guidance Control and Dynamics, 1997. **20**(6): p. 1181-1189.

[4] Ko, J., A.J. Kurdila, and T. Strganac, *Stability and control of a structurally nonlinear aeroelastic system.* Journal of Guidance Control and Dynamics, 1998. **21**: p. 718-725.

[5] Block, J.J. and T.W. Strganac, *Applied active control for a nonlinear aeroelastic structure.* Journal of Guidance Control and Dynamics, 1998. **21**(6): p. 838-845.

[6] Ko, J., T.W. Strganac, and A.J. Kurdila, *Adaptive Feedback Linearization for the Control of a Typical Wing Section with Structural Nonlinearity.* Nonlinear Dynamics, 1999. **18**(3): p. 289-301.

[7] Strganac, T., J. Ko, and D. Thompson, *Identification and control of limit cycle oscillations in aeroelastic systems.* Journal of Guidance Control and Dynamics, 2000. **23**(6): p. 1127-1133.

[8] Platanitis, G. and T.W. Strganac, *Control of a nonlinear wing section using leading- and trailing-edge surfaces.* Journal of Guidance Control and Dynamics, 2004. **27**(1): p. 52-58.

[9] Jiffri, S., et al., *Experimental Nonlinear Control for Flutter Suppression in a Nonlinear Aeroelastic System.* Journal of Guidance, Control, and Dynamics, 2017. **40**(8): p. 1925-1938.

[10] Pototzky, A., et al., *Calculating time-correlated gust loads using matched filter and random process theories*. Vol. 28. 1991.

[11] Kanda, A. and E. Dowell, *Worst-Case Gust-Response Analysis for Typical Airfoil Section with Control Surface*. Vol. 42. 2005. 956-962.

[12] Khodaparast, H. and J. Cooper, *Rapid Prediction of Worst-Case Gust Loads Following Structural Modification*. Vol. 52. 2014. 242-254.

[13] Khodaparast, H., et al., *Efficient Worst Case 1-Cosine Gust Loads Prediction*. Vol. 2. 2012. 33.

[14] Khodaparast, H., et al., *The Effects of Structural Nonlinearity on the Dynamic Response to Aeroelastic Gust Models*. 2016.

[15] Matas, L.G., et al., *Worst-case gust loads prediction with the effects of local structural nonlinearity*, in *AIAA Scitech 2019 Forum*.

[16] Ardelean, E.V. and R.L. Clark. *V-stack piezoelectric actuator*. in *SPIE Smart Structures and Materials*. 2001. SPIE.

[17] Ardelean, E.V., et al., *Active Flutter Control with V-stack Piezoelectric Flap Actuator.* Journal of Aircraft, 2006. **43**(2): p. 482-486.

[18] Da Ronch, A., et al., *A nonlinear controller for flutter suppression: from simulation to wind tunnel testing*, in *AIAA Science and Technology Forum and Exposition (13-17 Jan)*. 2014: National Harbor, MD.

[19] Theodorsen, T., *General theory of aerodynamic instability and the mechanism of flutter.* NACA Report no. 496, 1935: p. 413-433.
[20] Edwards, J.W., H. Ashley, and J.V. Breakwell, *Unsteady aerodynamic modeling for arbitrary motions.* AIAA Journal, 1979. **17**(4): p. 365-374.
[21] Fichera, S., S. Jiffri, and J.E. Mottershead, *Design and Wind Tunnel Test of a MODular Aeroelastic FLEXible Wing (MODFLEX)*, in *Proceedings of the International Conference on Noise and Vibration Engineering ISMA*. 2016: (Leuven, Belgium, September 2016).
[22] Wood, K.T., et al., *A New Gust Generator for a Low Speed Wind Tunnel: Design and Commissioning*, in *55th AIAA Aerospace Sciences Meeting*. 2017, American Institute of Aeronautics and Astronautics.

COPYRIGHT STATEMENT